



Synthesis of Fluorescent Nitrogen and Phosphorous Co-doped Carbon Quantum Dots for Sensing of Iron, Cell Imaging and Antioxidant Activities

Aschalew Tadesse¹ · Neway Belachew² · Mebrahtu Hagos³ · Keloth Basavaiah⁴

Received: 17 December 2020 / Accepted: 2 February 2021 / Published online: 2 March 2021

© The Author(s), under exclusive licence to Springer Science+Business Media, LLC part of Springer Nature 2021

Abstract

Carbon quantum dots (CQD) as the result of their exceptional physical and chemical properties show tremendous potential in various field of applications like cell imaging and doping of CQDs with elements like nitrogen and phosphorous increase its fluorescence property. Herein, we have synthesized fluorescent nitrogen and phosphorous codoped carbon quantum dots (NPCQDs) via a one-pot hydrothermal method. Sesame oil, L-Aspartic acid, and phosphoric acid were used as carbon, nitrogen, and phosphorous sources, respectively. UV-Vis spectrophotometer, fluorescence spectrometer, Fourier transform infrared spectrometer (FTIR), X-ray diffraction spectrometer (XRD), field emission scanning microscopy (FESEM), and transmission electron microscopy (TEM) were employed to characterize the synthesized fluorescent NPCQDs. The as-synthesized NPCQDs with a particle size of 4.7 nm possess excellent water solubility, high fluorescence with high quantum yield (46%), high ionic stability, and resistance to photobleaching. MTT assay indicated the biocompatibility of NPCQDs and it was used for multicolor live-cell imaging. Besides, the NPCQDs show an effective probe of iron ions (Fe^{3+}) in an aqueous solution with a high degree of sensitivity and selectivity. The DPPH assay showed its good antioxidant activity.

Keywords Sesame oil · L-aspartic acid · NPCQDs · Fe^{3+} ions probe · Antioxidant · Multicolor cell imaging

Introduction

Iron (Fe^{3+}) is one of the essential trace elements in living organisms since it has an important role in enzyme catalysis, cellular metabolism, a cofactor in enzyme-based reactions, and oxygen transport in hemoglobin [1–6]. The presence of Fe^{3+} above the maximum permissible level or in deficiency can disturb the cellular homeostasis, and result in various diseases, such as anemia, arthritis, intelligence decline, heart

failure, diabetes, and cancer [7–12]. Moreover, the presence of excess Fe^{3+} ions in water confronts the water quality by introducing bad odor and color. Therefore, detecting Fe^{3+} in living organisms and water is important from a health perspective. In recent time, detection of Fe^{3+} ion level using carbon quantum dots based materials as the fluorescent probe has got intense attention [13–16].

Since its accidental discovery in 2004 by Xu et al. [17] at the time of purifying single-walled carbon nanotubes (SWCNTs) fabricated by arc-discharge methods, carbon quantum dots has been inspiring intensive research efforts. Sun et al. have reported the planned synthesis of CQD for the first time in 2006 [18, 19]. Since then several research articles reported showing the fascinating properties of discrete, quasi-spherical CQDs with sizes below 10 nm [20–22]. CQDs can be amorphous or nanocrystalline with sp^2 carbon clusters and some diamond-like structures formed by sp^3 carbons [23, 24]. CQDs are rich with carboxyl and hydroxyl functional groups at their surface, thus imparting them with excellent water solubility and the suitability for subsequent functionalization with various organic, polymeric, inorganic, or biological species [20, 22, 25]. The presence of

✉ Aschalew Tadesse
asche.best@gmail.com

¹ Department of Applied Chemistry, Adama Science and Technology University, Adama, Ethiopia

² Department of Chemistry, Debre Berhan University, Debre Berhan, Ethiopia

³ Faculty of Natural and Computational Sciences, Woldia University, 400 Woldia, Ethiopia

⁴ Department of Inorganic and Analytical Chemistry, Andhra University, Visakhapatnam 530003, India

the surface states greatly modifies the optical properties of CQDs. Such surface states can be originated from the presence of vacancies, impurities, dopants, and chemisorbed species [26]. The optical properties can be effectively improved as CQDs doped with heteroatoms due to the incorporation of the element into the nanocrystal core and/or effective surface passivation [27, 28]. The most common doping atoms are nitrogen [29], sulfur [30], and other elements like boron, phosphorous, copper, and gadolinium have also been used [31–33].

Hydrothermal method is one of the best method for synthesis of fluorescent CQDs using different precursors [34, 35]. Nowadays, several researchers have strived for the preparation of fluorescent CDs using facile and less harmful organic chemicals. However, the synthesis of CQDs from natural and cheaply available precursors have shown an indispensable for the sustainability for practical applications. Various natural products such as orange juice [36], *Saccharum officinarum* juice [37], protein [38], carbohydrate [39], and others were used as a precursor for the preparation of photoluminescent CQDs. The quantum yield and fluorescent properties of CQDs are varied with different sources.

Hence, this study is intended to synthesis fluorescent nitrogen and phosphorous co-doped carbon quantum dots (NPCQDs) using easily available sesame oil as carbon source, L-Aspartic acid as nitrogen source, and diluted phosphoric acid as phosphorous source. The synthesized NPCQDs were characterized and used for sensing of iron (III) ions in solution and live-cell imaging. Besides, the antioxidant activity was investigated using DPPH assay method, and the result showed that the prepared NPCQD is an effective antioxidant.

Experimental Section

Chemicals and Reagents

Sesame oil was purchased from the local store nearby Adama Science and Technology University, Ethiopia, and NPCQDs were synthesized using sesame oil as carbon source through the hydrothermal method. L-Aspartic acid was obtained from HiMedia Laboratories, Mumbai, India. Orthophosphoric acid was obtained from Merck life science, Mumbai, India. Throughout the study, analytical grade reagents were used without any purification. The deionized water was used throughout experiment.

Preparation of NPCQDs

In a typical procedure, 15 mL of clear sesame oil, and 0.20 g of L-Aspartic acid dissolved in 10 mL of 0.1 M H_3PO_4 were taken in 100 mL Teflon-lined stainless steel autoclave. The autoclave was placed in a furnace at 200 °C for 8 h. The black paste was

collected after it cools down to room temperature then dissolved in 25 mL of water. The brown solution was centrifuged for 15 min at 3000 RPM to remove insoluble matter and then centrifuged at 12000 RPM for 20 min repeatedly three times to remove larger size particles. The resulting NPCQDs solution was kept in a refrigerator at 4 °C for further use.

Characterizations

The morphology and microstructures of the synthesized NPCQDs were determined by TEM and high-resolution transmission electron microscopy (HRTEM, Jeol/JEM 2100, LaB6) operated at 200 kV. Elemental composition of the samples were determined using field emission scanning electron microscopy (FESEM, Zeiss Ultra-60) equipped with X-ray energy dispersive spectroscopy (EDS). XRD pattern were recorded using PANalytical X'pert pro diffractometer using $Cu\alpha_1$ radiation (45 kV, 1.54056 Å; scan rate of 0.02 degree/s). FTIR spectra were obtained over the range of 500–4000 cm^{-1} using FTIR Spectrometer (Bruker). Fluorescence properties of the samples were measured with Fluoromax-4 Spectrofluorometer (HORIBA Scientific). UV–Vis absorption spectra were obtained using a UNICAM UV 500 (Thermo Electron Corporation).

Quantum Yield

Quinine sulfate in 0.1 M sulphuric acid with the quantum yield of 54% at 365 nm was used as a reference to determine quantum yield of the prepared fluorescent NPCQDs following the reported protocol [40]. The UV–Vis absorption at 365 nm and PL emission spectra after excitation at 365 nm of NPCQDs and reference was measured, respectively where absorbance were kept under 0.05 to minimize the re-absorption effects,.

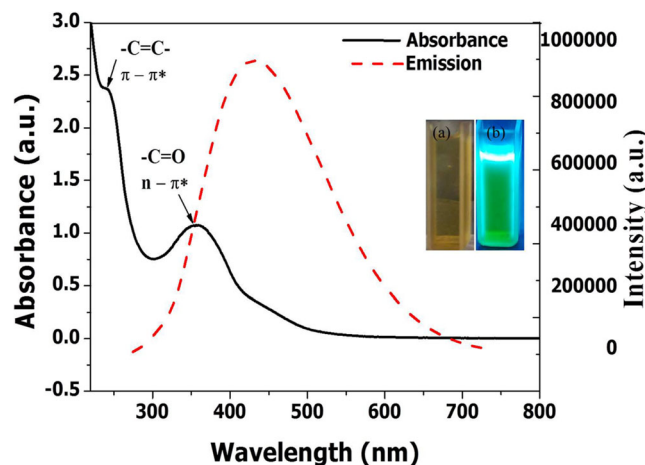


Fig. 1 (Solid line) UV-Vis absorption spectrum of NPCQDs (inset NPCQDs solution (a) under daylight (b) under ultraviolet radiation) and (Broken line) Emission spectra at 360 nm Excitation

$$QY_{\text{samp}} = QY_{\text{ref}} \left(\frac{I_{\text{samp}}}{I_{\text{ref}}} \right) \left(\frac{A_{\text{ref}}}{A_{\text{samp}}} \right) \left(\frac{n_{\text{samp}}^2}{n_{\text{ref}}^2} \right) \quad (1)$$

where QY_{samp} and QY_{ref} are quantum yield of sample and reference, I_{samp} and I_{ref} are emission intensity, A_{samp} and A_{ref} are UV-Vis absorbance, n_{samp} and n_{ref} are refractive index of sample and reference, respectively.

Quantitative Determination of Iron (III) Ions and Selectivity Study

For the quantitative determination of iron (III) ions (Fe^{3+}), NPCQDs solution with UV-Vis absorbance of 0.04 was prepared in a pH 7.4 phosphate buffer solution. 3 mL of this solution was taken in vials and mixed with 200 μL of different concentrations of Fe^{3+} solution then aged for 5 min to attain equilibration. The FL spectra of the solutions were recorded. The selectivity for a Fe^{3+} was confirmed by adding other metal ions solutions (Na^+ , K^+ , Ag^+ , Mg^{2+} , Cu^{2+} , Ni^{2+} , Ca^{2+} , Cd^{2+} , Zn^{2+} , Fe^{2+} , Ba^{2+} , Pb^{2+} , Al^{3+}) instead of Fe^{3+} in a similar way.

Cytotoxicity Study

Human breast adenocarcinoma (MCF7) cell was used as a strain to evaluate invitro cytotoxicity of NPCQDs

following MTT Assay method [13]. The cells were cultured in 96-well tissue culture plates at a density of 1×10^4 cells per well following the same procedure used by Aschalew et al. [41]. After adhering, the cells were incubated with a medium containing different doses of NPCQDs for 24 h. The medium from each well was removed after incubation and then the cells were washed using phosphate buffered solution. A fresh medium containing 10 μL of 0.5 mg mL^{-1} solution of MTT was added to each well and incubated for 4 h and then the medium was replaced with DMSO (150 μL) followed by shaking for 15 min to dissolve the formazan crystals. Multimode microplate reader (Biotek, Cytation3) was used to record the absorbance of each well at 570 nm. The untreated cells were used as controls for calculating the relative percentage of cell viability from the following equation:

$$\begin{aligned} \% \text{Cell viability} &= \left(\frac{A_{570} \text{ in treated sample}}{A_{570} \text{ in control sample}} \right) \\ &\times 100\% \end{aligned} \quad (2)$$

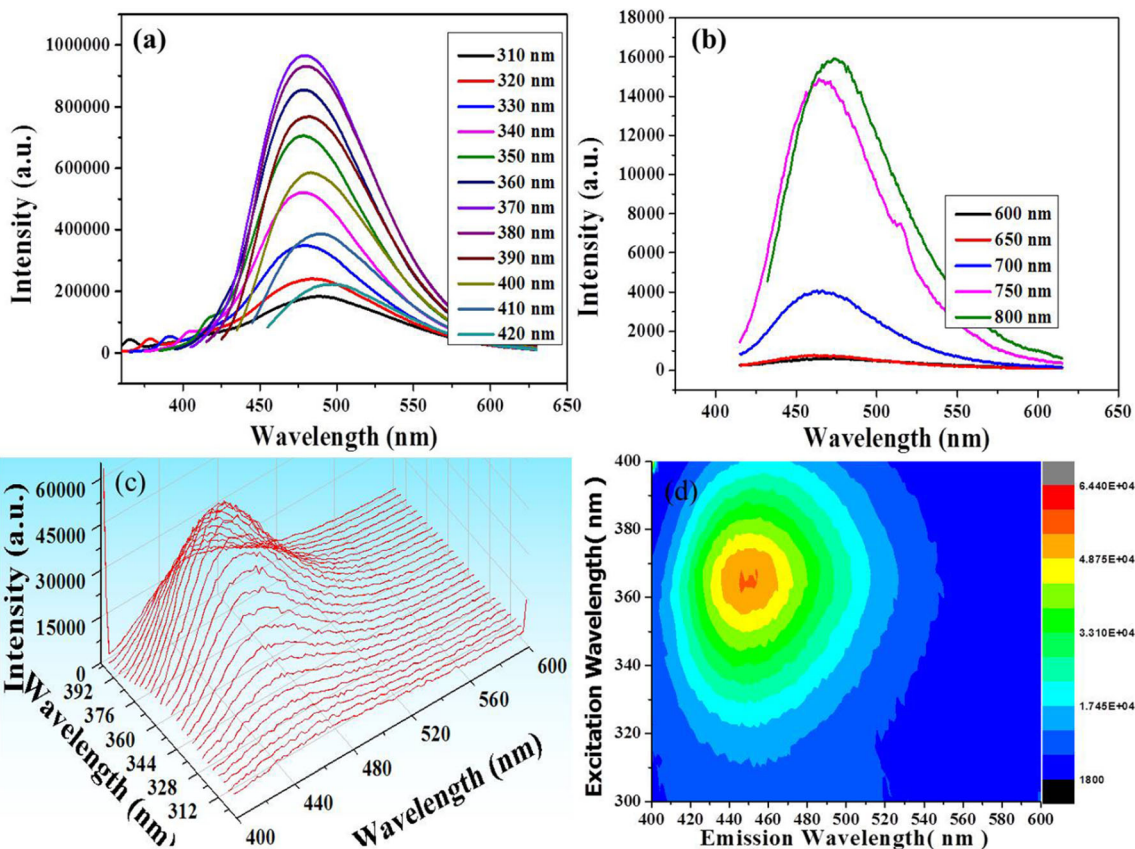


Fig. 2 a Fluorescence emission spectra with excitation wavelengths from 310 nm to 420 nm of NPCQDs, b Up-converted Fluorescence emission spectra of NPCQDs at excitation wavelengths from 600 nm to 800 nm, c

3D Fluorescence Spectra of NPCQDs (Excitation with radiation from 300 nm to 400 nm and Corresponding Emission), (d) Excitation and emission contour map of NPCQDs

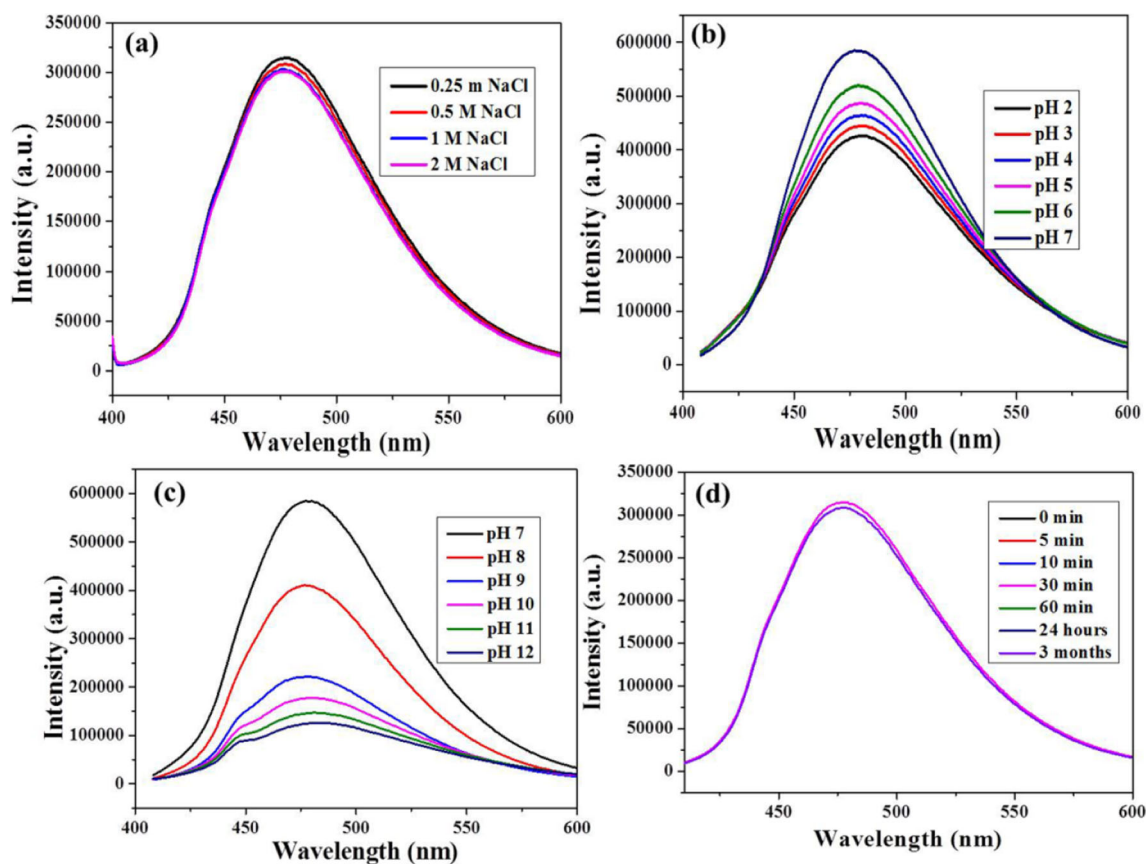


Fig. 3 a Fluorescence intensity of NPCQDs at excitation wavelength of 365 nm indicating ionic strength with NaCl solution of concentration 0.25 M to 2 M, b pH effect in acidic media with pH of 7 to 2, c pH effect in basic media with pH of 7 to 12, d stability after irradiation at different time

Multicolor Cell Imaging

Fluorescent imaging ability of NPCQDs was tested using MCF7 Cells [42]. The cells were seeded in 6-well culture plates at 10^5 cells per well density in DMEM containing 10% Fetal bovine serum (FBS) and incubated for 24 h at 37 °C and 5% CO₂ following the same procedure used by Aschalew et al. [41]. Then the medium was replaced with a fresh medium containing 0.025 mg mL^{-1} NPCQDs and further incubated for 6 h. After that, the cells were washed three times with PBS to remove extracellular NPCQDs, fixed with paraformaldehyde (4%), and mounted using glycerol (50%). Zeiss LSM 510 Meta confocal Microscopy was used to record fluorescent images at laser excitations of 405, 488, and 561 nm.

Antioxidant Activity of NPCQDs

Antioxidant activity of NPCQDs was assessed by 2, 2-diphenyl-1-picrylhydrazyl (DPPH) assay methods with some modification [43, 44]. In a typical process, 2 mL (100 μM) of DPPH prepared by using ethanol as solvent was taken, and 1 mL of different concentrations of NPCQDs solution were mixed and reaction mixture sonicated and kept in dark for 1 h.

Time-dependent radical scavenging of NPCQDs was tested by mixing 2 mL (100 μM) of DPPH solution and 1 mL of 100 $\mu\text{g mL}^{-1}$ of NPCQDs solution and then UV-Vis absorbance of mixture measured after different time of reaction. The deep violet color of DPPH solution gradually changed to pale yellow in the presence of NPCQDs. This property allows visual monitoring of the reaction, and UV-Vis absorbance of reaction solution measured and the radicals scavenging efficiency of NPCQDs was determined from the change in the percentage of absorption at 517 nm. DPPH scavenging efficiency is calculated using the following equation:

$$\text{Radical Scavenging (\%)} = 100 \times (A_c - A_s) / A_c \quad (3)$$

Where A_c and A_s are the absorbances of control and sample at 517 nm, respectively.

Result and Discussions

Characterization

To explore the optical properties, the absorption and fluorescence emission spectra were recorded and as it is depicted in Fig. 1 (solid line), the UV-Vis absorption spectra show two

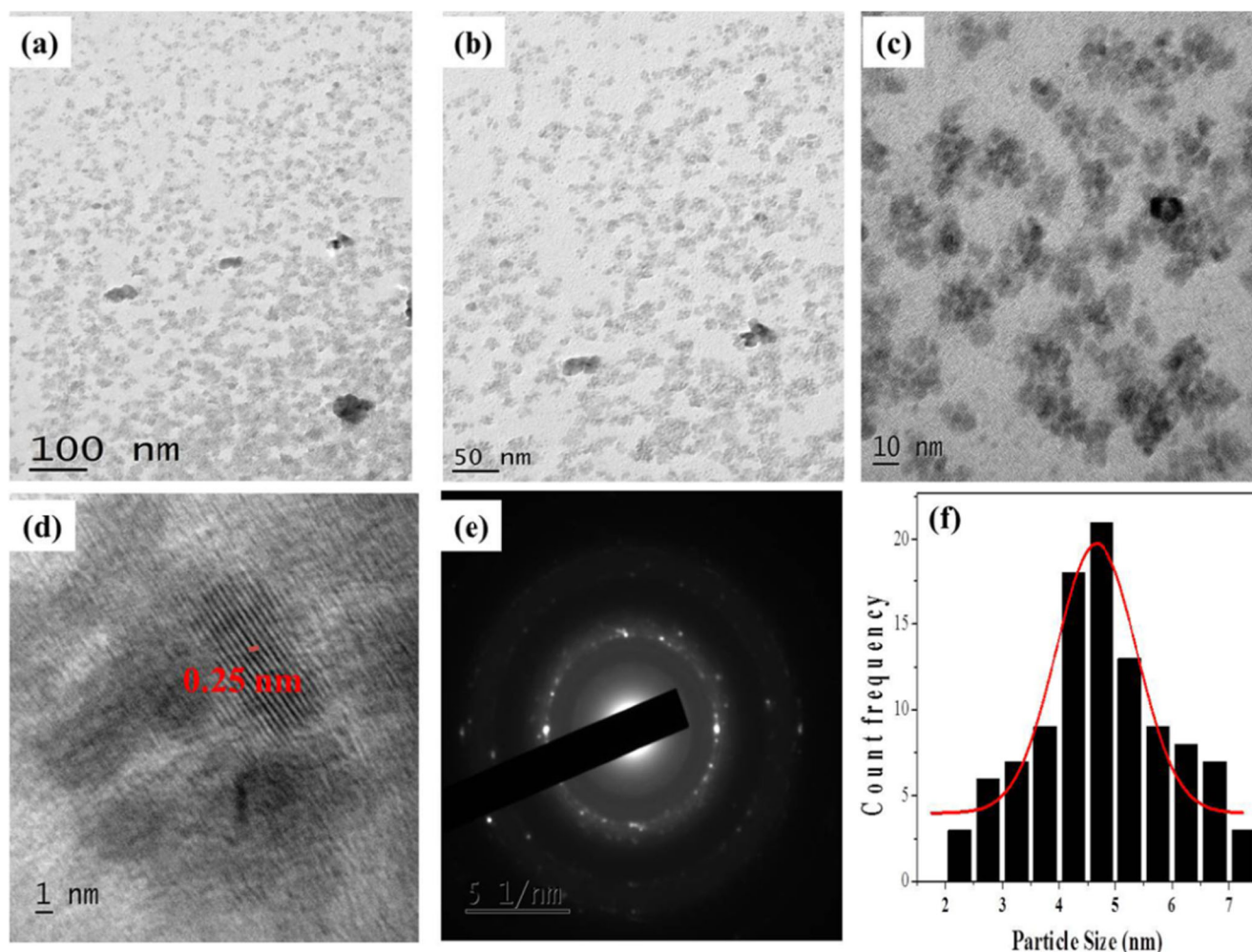


Fig. 4 a, b and c Representative TEM d HRTEM images, e SAED and f particle size distribution histogram of NPCQDs

peaks at 353 nm and shoulder peak at 251 nm, which correspond to $n-\pi^*$ transitions of C=O, C-N and C-P bonds and $\pi-\pi^*$ transition of C=C bonds, respectively [45, 46]. As shown in Fig. 1 inset (a) the solution has yellowish-brown color under daylight and it became bright green under long wavelength ultraviolet irradiation indicating the green fluorescence of the synthesized carbon quantum dots (Fig. 1 inset b). The excitation-emission spectra of the synthesized NPCQDs is indicated in Fig. 1 (broken line) which shows the fluorescence at maximum emission wavelength of 479 nm after excitation at 370 nm. The narrow size distribution of the prepared NPCQDs can be revealed from full-width at half maximum (FWHM) value of 86 nm [21, 47].

A detailed fluorescence study was carried out by exciting the as-synthesized NPCQDs at different excitation wavelengths. As shown in Fig. 2, the sample shown strong fluorescence with symmetrical peaks and emission wavelength were not depending on the excitation wavelength. However, the emission intensity increased as excitation wavelength increased from 310 nm to 370 nm, and maximum emission intensity obtained at excitation wavelength of 370 nm

(Fig. 2a). Further increase in excitation wavelengths resulted in decrease of emission intensity. This variation in emission intensity with excitation wavelength is because of different energy levels incorporated into the NPCQDs by different surface groups such as C-O, C=O, O=P-OH, C-N-H and O=C-OH and it indicated that the fluorescence originated from quantum confinement effect [48]. In addition to down-converted fluorescence emission, as shown in Fig. 2b, NPCQDs show up-converted fluorescence emission with emission wavelength at 468 nm when excited at higher wavelength radiation. 3D fluorescence emission spectra of the NPCQDs with excitation wavelengths varying from 300 nm to 400 nm in 4 nm increments is shown in Fig. 2c and the result indicated symmetrical emission peaks. Excitation and emission contour map of NPCQDs (Fig. 2d) depicted multicolour emission. The fluorescence emission of NPCQDs may be due to π -plasmon absorption in the core carbon nanoparticles and it may also be affected by surface chemistry of the as synthesized nanomaterials [49, 50]. The analysis result of the as synthesized NPCQDs has shown high FL quantum yield of about 46% which is relatively high

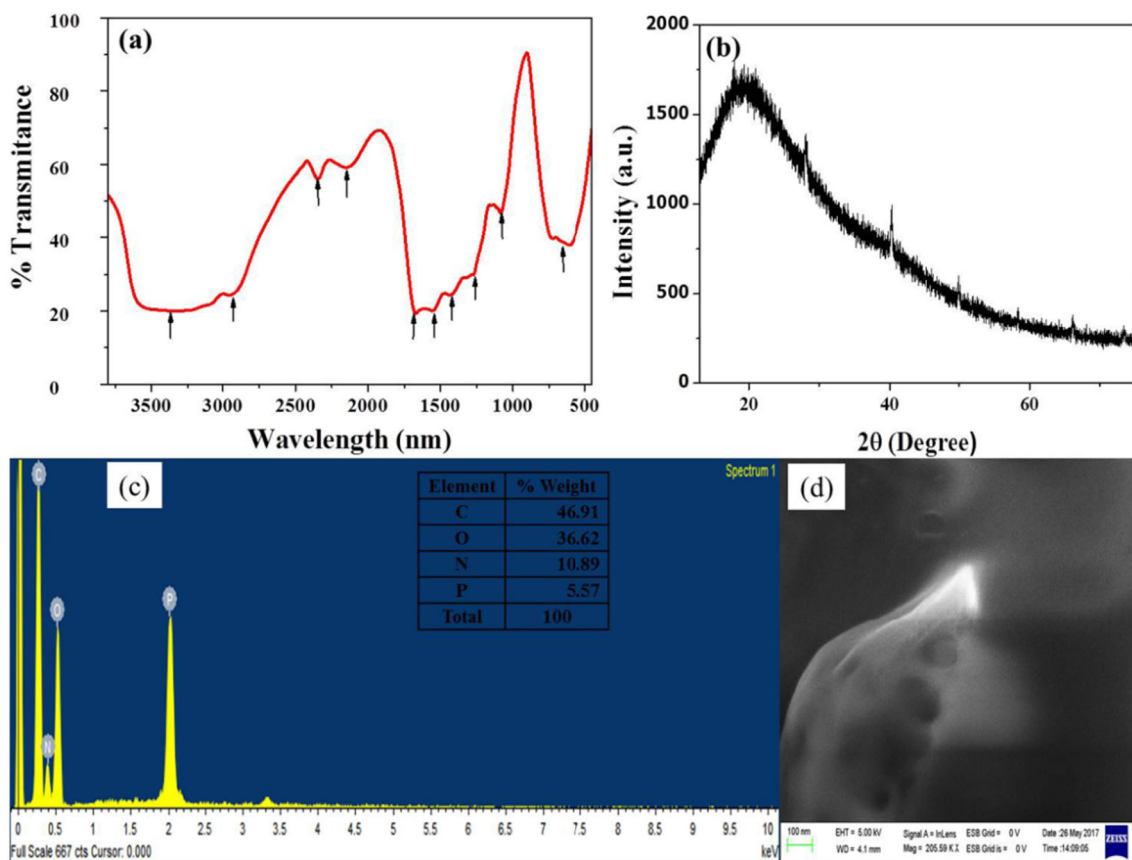


Fig. 5 **a** FTIR spectrum, **b** XRD peak of NPCQDs, **c** EDS spectrum (inset table elemental composition of NPCQDs) and **d** FESEM image

compared to carbon quantum dots derived from natural products [51–53].

Fluorescence stability of the synthesized NPCQDs toward ionic strength was studied by changing concentration of sodium chloride (0.25 M to 2 M NaCl) and the result indicated that concentration of salt has no significant effect on fluorescence of NPCQDs (Fig. 3a). Changing pH of NPCQDs changed the fluorescence intensity of the NPCQDs but has no effect on emission wavelength. As pH decreased from 7 to 2, the FL intensity increased (Fig. 3b) and as pH increased from 7 to 12, the FL intensity decreased (Fig. 3c) and the change in emission intensity may be due to protonation and deprotonation of the NPCQDs at different media [48]. Moreover, the NPCQDs have revealed high photostability in that neither no shift in emission wavelength nor no significant reduction in FL intensity as the material irradiated with ultraviolet radiation from 1 min to 24 h (Fig. 3d) and after three months storage there is no change in fluorescence intensity.

Morphology and structural properties of NPCQDs were determined using TEM and HRTEM (Fig. 4a–e). ImageJ software was used to calculate the particle size of the as prepared NPCQDs from TEM image and the size distributed in diameter range of 2–8 nm with an average of 4.7 nm based on statistical analysis of about 100 dots (histogram in Fig. 4f). The holes in the selected area electron diffraction (SAED)

(Fig. 4e) indicated the particle formation and the graphitic amorphous nature of the NPCQDs. The as synthesized NPCQDs exhibit a lattice spacing of 0.25 nm (Fig. 4d) which is close to the (102) facet of sp^2 graphitic carbon [54, 55]. X-ray diffraction (XRD) patterns (Fig. 5b) showed a broad and intense diffraction peak centered at $2\theta = 23^\circ$ and weak peak at $2\theta = 42^\circ$ which assigned to (002) and (101) diffraction pattern of graphitic carbon which indicated the amorphous nature of the NPCQDs and is in accordance with previous structure analysis on disordered amorphous graphitic carbon quantum dots [56].

Fourier transform infrared spectroscopy (FTIR) analysis was used to get information about the surface functional group of NPCQDs. The FTIR spectrum depicted in Fig. 5a confirmed the presence of different functional groups in the synthesized NPCQDs. There is a broad overlapping strong band in the range 3070–3600 cm^{-1} that can be assigned to the carboxyl O–H and amine N–H bonds stretching vibration [57]. The C–O bond vibrational band at 1076 cm^{-1} confirmed the presence of primary –OH groups on the surface of NPCQDs. The appearance of bands at 2934 cm^{-1} confirmed presence of aliphatic C–H bonds. The weak and broad band at 2154 cm^{-1} and weak sharp band at 2348 cm^{-1} indicated the presence of O=P–OH bond [58]. The band at 1271 cm^{-1} indicated the presence of C–N bond. The band at 1544 cm^{-1} can be

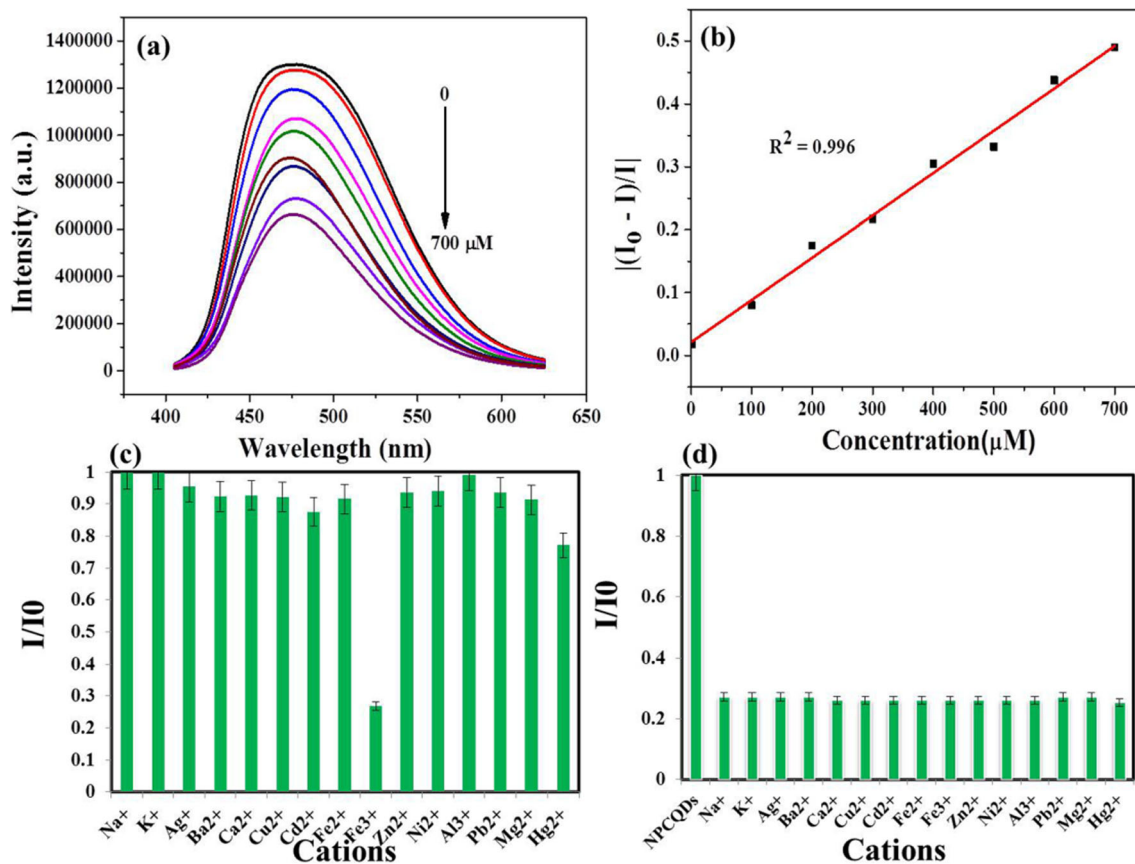


Fig. 6 **a** Fluorescence spectra of NPCQDs solution in the presence of different concentrations of Fe³⁺ and **b** plot of concentration versus $(I_0 - I)/I$, **c** Fluorescence quenching response of NPCQDs to different metal ions,

d Specific FL quenching response of NPCQDs to Fe³⁺ ions in presence of other cations

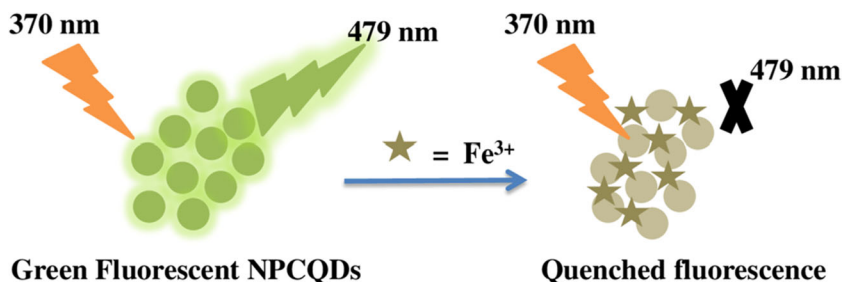
assigned to N-H vibration and deformation which indicated the presence of amino functional group [59]. The band at 1668 cm⁻¹ indicated asymmetric and symmetric bond vibration of carboxylic C=O functional group [60]. Moreover, the presence of stretching and bending vibrational bands for C-H and stretching vibrations for C=C in aromatic hydrocarbons at 3060, 770 and 1434 cm⁻¹ confirmed the presence of the aromatic skeleton (sp² hybridized carbon) in the prepared NPCQDs [61]. The band at 610 cm⁻¹ due to out of plane bending of P-OH confirmed the presence of P atom in NPCQDs [62]. Therefore, the FTIR result indicated the presence of nitrogen and phosphorous in the prepared NPCQDs.

Shining surface paper sheet layer like FESEM images in Fig. 5d indicated the graphitic amorphous nature of NPCQDs [41]. Result from elemental composition analysis of FESEM/EDS spectrum (Fig. 5c) revealed the presence of C, O, N and P in the as synthesized material indicating well formation of nitrogen, phosphorous co-doped carbon quantum dots.

Fluorescence Quantitative Assay of Fe³⁺ Ions

In recent time, fluorescence quenching based selective detection of metal ions has become the interesting research area [13]. Selectivity study of the fluorescence sensing of Fe³⁺ ions

Scheme 1 Scheme showing Fluorescence quenching of NPCQDs by Fe³⁺ ions



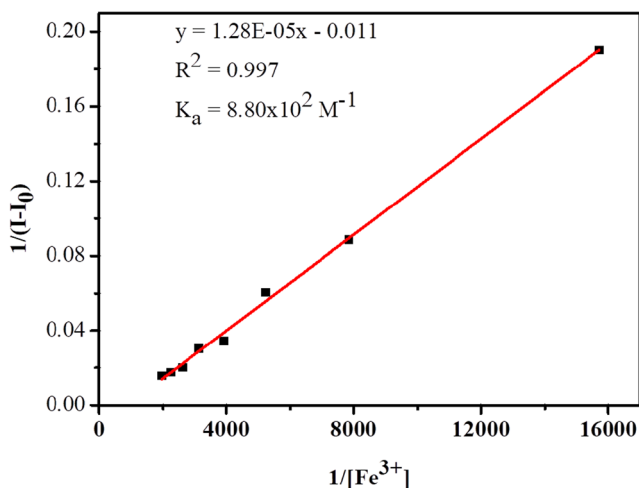
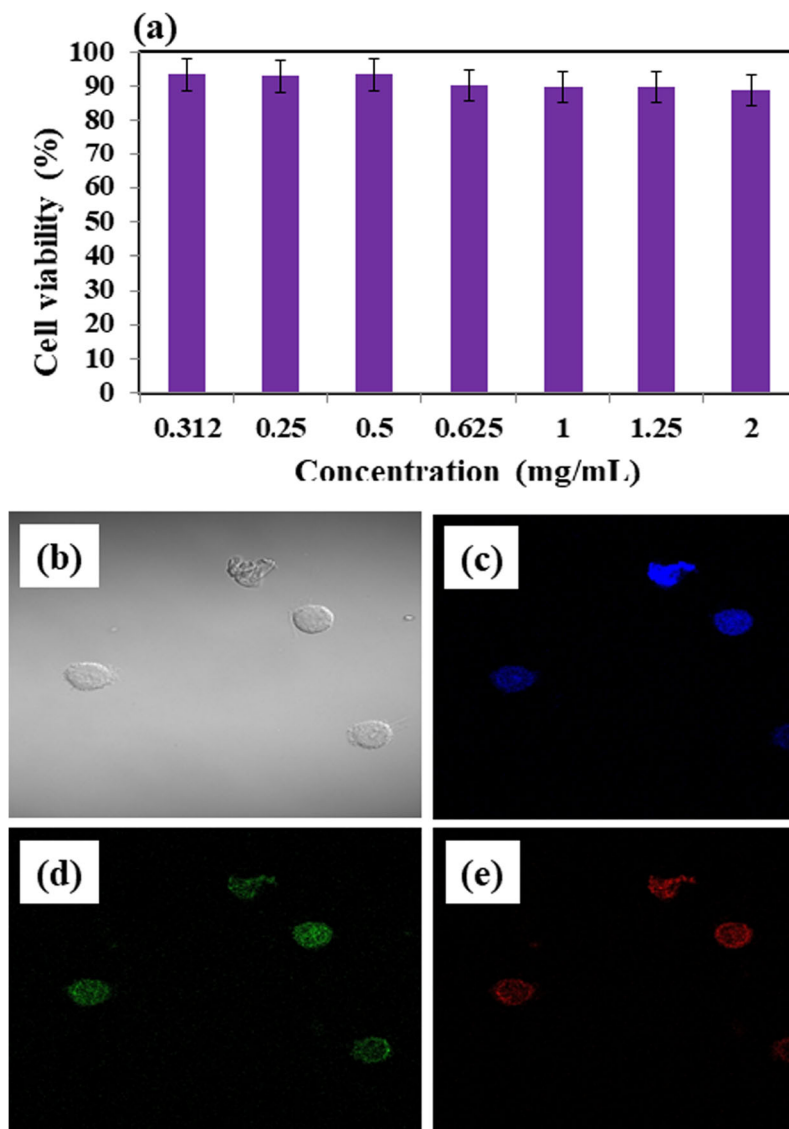


Fig. 7 Benesi-Hildebrand plot of $1/(I-I_0)$ as a function of $1/[Fe^{3+}]$

using NPCQDs over other competing ions (Na^+ , K^+ , Mg^{2+} , Mn^{2+} , Cu^{2+} , Ni^{2+} , Ca^{2+} , Co^{2+} , Cd^{2+} , Zn^{2+} , Fe^{2+} , Sn^{2+} , Ba^{2+} , Hg^{2+} , Pb^{2+} , Al^{3+}) were tested separately by adding 30 μL of 10^{-4} M solution of cations to 3 mL of phosphate buffered NPCQDs solutions and fluorescence recorded. Fe^{3+} and Hg^{2+} showed fluorescence quenching while other cations quenching were insignificant (Fig. 6c). Interference of the above cations with Fe^{3+} were investigated by taking 30 μL of 10^{-4} M solution of cations with 30 μL of 10^{-4} M of Fe^{3+} ions and then fluorescence recorded. The result (Fig. 6d) confirmed that the presence of the cations not interfere with fluorescence sensing of Fe^{3+} .

The fluorescence sensing performance of the NPCQDs based on fluorescence probe was assessed by adding different concentrations of Fe^{3+} (0–400 μM) in to the NPCQDs solution. The fluorescence of NPCQDs was quenched in presence

Fig. 8 a Cell viability of MCF7 cells by MTT assay **b, c, d** and **e** confocal fluorescence microscopic images of NPCQDs labelled MCF7 cells under bright field, 405 nm excitation, 488 nm excitation and 561 nm excitation, respectively



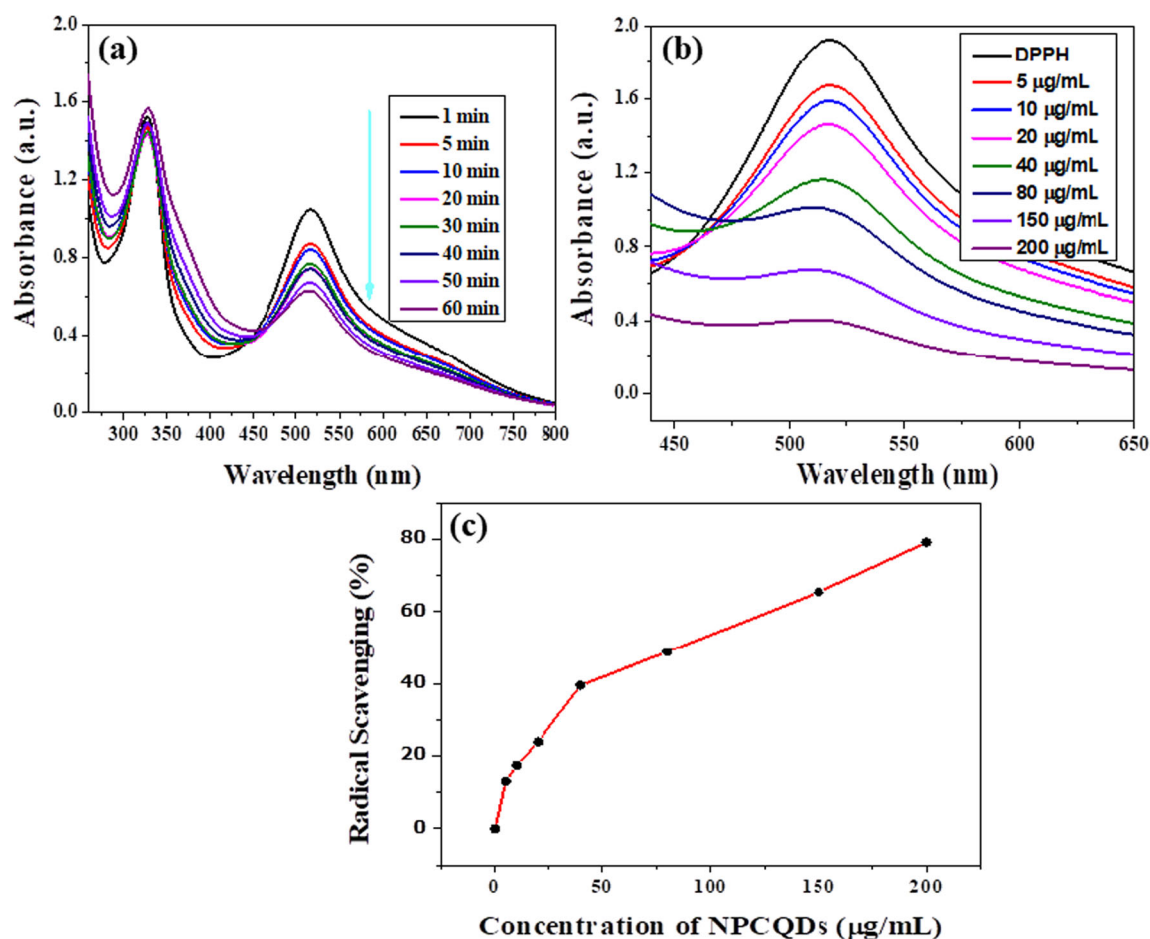


Fig. 9 **a** UV-Vis absorption spectra of DPPH solution in presence of 100 µg/mL NPCQDs at different time of reaction, **b** UV-Vis absorption spectra of DPPH solution in different concentration of NPCQDs at fixed 1 h of reaction and **c** plot of concentration of NPCQDs versus % radical scavenging

of Fe^{3+} ion (Scheme 1) and the fluorescence quenching intensity depend on concentration of Fe^{3+} . Fluorescence spectra in the presence of various concentrations of Fe^{3+} in NPCQDs are shown in Fig. 6a. As concentration of Fe^{3+} increased, the fluorescence intensity of the NPCQDs was decreased gradually. Correlation between the fluorescence quenching of NPCQDs and concentration of Fe^{3+} was obtained as shown in Figs. 6b. The fluorescence quenching efficiency can be further described by the Stern–Volmer plot with a perfect linear correlation coefficient of 0.992 in the linear range of Fe^{3+} concentrations from 20 to 200 µM [63]. K_{SV} of quenching agent of Fe^{3+} was only 1.35×10^{-3} , far more less than that of dynamic quenching (commonly in the range of 10^2 – 10^3), and therefore, the quenching mechanism is a static quenching mechanism [64] (Fig 7).

The Stern–Volmer equation thus achieved was:

$$I_0/I = 1.35 \times 10^{-3} [\text{Fe}^{3+}] + 1.07057 \quad (4)$$

where I_0 and I were the fluorescence intensities of NPCQDs in the absence and presence of Fe^{3+} and $[\text{Fe}^{3+}]$ represented the concentration of Fe^{3+} .

The binding stoichiometry between NPCQDS and Fe^{3+} were determined by determining binding constant using Benesi-Hildbrand plot [65] after plotting $1/(I-I_0)$ versus $1/[\text{Fe}^{3+}]$ from the equation:

$$1/(I-I_0) = 1/\{K_b(I-I_{\min})[\text{Fe}^{3+}]\} - 1/(I_0-I_{\min}) \quad (5)$$

Where, I and I_0 are the emission intensity of NPCQDs in presence and absence of Fe^{3+} ion and I_{\min} is the minimum intensity of NPCQDs in presence of Fe^{3+} ion. The binding constant, K_b was determined by dividing intercept for slope of plot $1/(I-I_0)$ vs $1/[\text{Fe}^{3+}]$. K_b value was $8.80 \times 10^2 \text{M}^{-1}$ which indicated good binding attraction between the fluorescent NPCQDs and Fe^{3+} ions [66].

Cell Cytotoxicity and Live Cell Imaging

As a fluorescent probe, the potential use of the as synthesized NPCQDs was evaluated for bioimaging and biolabeling in live cells. The inherent cell viability of NPCQDs was assessed in human breast adenocarcinoma (MCF7) cells through MTT assay. NPCQDs exhibited extremely low cytotoxicity with

cell viability of about 89% even at relatively high concentration of 2 mg mL⁻¹ and at 24 h of exposure time (Fig. 8a). In addition, the bright-field optical images validated that there were no morphological change after the NPCQDs application, indicating that the as-synthesized NPCQDs has good biocompatibility.

As a bioimaging probe, the potential application of the prepared NPCQDs was assessed by treating MCF7 Cells with 0.025 mg/mL of sesame oil derived NPCQDs. After incubation for 4 h, the MCF7 were washed to remove extracellular NPCQDs and observed under fluorescent microscopy at laser excitations of 405, 488 and 561 nm. We found that the labelled cells were brightly illuminated with multicolor images due to strong fluorescence emitting from the NPCQDs distributed in the cytosol (Fig.8b-e) and exhibited blue, green and red fluorescence corresponding to the laser excitation at 405 nm, 488 nm and 561 nm. The results indicated that the highly water soluble, photostable fluorescent sesame oil derived nitrogen and phosphorous co-doped carbon quantum dots can serve as an excellent fluorescent bioimaging probe.

Antioxidant Activities of NPCQDs

DPPH assay is a standard method which provides a way to evaluate antioxidant activity of materials. DPPH is a long-lived, nitrogen containing free radical that can be used as a free radical source and gets scavenged in the presence of antioxidant and has deep purple colour in solution, which turns yellow as soon as it interacts with an antioxidant. There are few promising reports concerning carbon dots antioxidant activity [44, 67]. In this study, we evaluated the antioxidant activity of NPCQDs using DPPH assay method in comparison to ascorbic acid as positive control. The gradual color change of DPPH solution from deep violet to pale yellow in presence of NPCQDs indicated the radical scavenging activity of NPCQDs. As shown in Fig.8a, in presence of 100 µg/mL of NPCQDs, as time increase from 1 min to 60 min the UV-Vis absorbance of DPPH solution at 517 nm decreased indicating that at longer contact time, more efficiency for radical scavenging. Antioxidant activity study using different concentration of NPCQDs at fixed time of 60 min indicated that as concentration increased, the radical scavenging capacity increased as shown in Fig.8b and c. Hence, the as synthesized NPCQDs can be used as good antioxidant materials (Fig 9).

Conclusions

In summary, a facile, environmentally green hydrothermal method was used to synthesis highly fluorescent nitrogen and phosphorous co-doped carbon quantum dots (NPCQDs) using sesame oil, L-Aspartic acid and phosphoric acid as carbon, nitrogen and phosphorous source, respectively.

Characterization result indicated that the synthesized NPCQDs have narrow size distribution, bright fluorescence with high quantum yield, pH dependent, highly ionic stable and photostable fluorescence. Investigation for application confirmed that the as synthesized NPCQDs can be used as promising probe for Fe³⁺ ions in aqueous media. MTT assay demonstrated that NPCQDs exhibited low cell toxicity and excellent biocompatibility. The multicolor live cell imaging of the NPCQDs was investigated and we conclude that the NPCQDs may be used as an eco-friendly fluorescent nanomaterial for potential multicolor imaging and sensing applications. The result from DPPH assay revealed that the prepared sesame oil derived NPCQDs is promising for antioxidant activity.

Acknowledgments Authors would like to thanks Adama Science and Technology University as well as Andhra University for allowing us to use laboratory facilities in the Universities.

Author Contributions All authors contribute equally to this work.

Data Availability All data generated or analysed during this study are included in this published article.

Declaration

Conflict of Interest The authors declare that the research was conducted in the absence of any commercial or financial relationships that could be construed as a potential conflict of interest.

References

1. Crichton R, Crichton RR, Boelaert JR (2001) *Inorganic Biochemistry of Iron Metabolism: From Molecular Mechanisms to Clinical Consequences*. John Wiley & Sons, Hoboken
2. Theil EC (2013) Iron, Biological Properties, Introduction to Iron Entries. *Encyclopedia of Metalloproteins* 1032–1032
3. De Visser SP, Kumar D (2011) *Iron-Containing Enzymes: Versatile Catalysts of Hydroxylation Reactions in Nature*. Royal Society of Chemistry, Cambridge
4. Rouault TA (2006) The role of iron regulatory proteins in mammalian iron homeostasis and disease. *Nat Chem Biol* 2:406–414
5. van Swelm RPL, Wetzels JFM, Swinkels DW (2020) The multifaceted role of iron in renal health and disease. *Nat Rev Nephrol* 16: 77–98
6. Zhang D-L, Ghosh MC, Rouault TA (2014) The physiological functions of iron regulatory proteins in iron homeostasis - an update. *Front Pharmacol* 5
7. Stoffel NU, Uyoga MA, Mutuku FM et al (2020) Iron Deficiency Anemia at Time of Vaccination Predicts Decreased Vaccine Response and Iron Supplementation at Time of Vaccination Increases Humoral Vaccine Response: A Birth Cohort Study and a Randomized Trial Follow-Up Study in Kenyan Infants. *Front Immunol* 11:1313
8. Rivella S, Crielgaard BJ (2014) Disorders of Iron Metabolism: Iron Deficiency and Iron Overload and Anemia of Chronic Diseases. *Pathobiology Hum Dis*:1471–1487

9. Moy RJD (2009) Nutritional Iron Deficiency in Early Childhood. *Iron Deficiency and Overload* 313–326
10. Lewis C-A, de Jersey S, Seymour M et al (2020) Iron, Vitamin B, Folate and Copper Deficiency After Bariatric Surgery and the Impact on Anaemia: a Systematic Review. *Obes Surg*. <https://doi.org/10.1007/s11695-020-04872-y>
11. Puntis J (2018) Iron deficiency. *Oxford Medicine Online*
12. Beattie RM, Mark Beattie R, Dhawan A, Puntis JW (2011) Iron deficiency. *Oxford Medicine Online*
13. Sun X, He J, Yang S et al (2017) Green synthesis of carbon dots originated from Lycii Fructus for effective fluorescent sensing of ferric ion and multicolor cell imaging. *J Photochem Photobiol B* 175:219–225
14. Wang F, Hao Q, Zhang Y et al (2016) Fluorescence quenchometric method for determination of ferric ion using boron-doped carbon dots. *Microchim Acta* 183:273–279
15. Hu Y, Gao Z (2019) Highly Photoluminescent Carbon Dots Derived from Discarded Chewing Gum: toward Multiple Sensing of pH, Ferric Ion, and Adenosine Triphosphate. *ChemistrySelect* 4: 12807–12814
16. Vashisht D, Sharma E, Kaur M et al (2020) Solvothermal assisted phosphate functionalized graphitic carbon nitride quantum dots for optical sensing of Fe ions and its thermodynamic aspects. *Spectrochim Acta A Mol Biomol Spectrosc* 228:117773
17. Sun Y-P, Zhou B, Lin Y et al (2006) Quantum-Sized Carbon Dots for Bright and Colorful Photoluminescence. *J Am Chem Soc* 128: 7756–7757
18. Liang G, Shi H, Qi Y et al (2020) Specific Anti-biofilm Activity of Carbon Quantum Dots by Destroying Biofilm Related Genes. *Int J Nanomedicine* 15:5473–5489
19. Xu X, Ray R, Gu Y et al (2004) Electrophoretic analysis and purification of fluorescent single-walled carbon nanotube fragments. *J Am Chem Soc* 126:12736–12737
20. Balding TR (2018) Carbon Quantum Dots for Bioimaging and Photocatalytic Improvement
21. Zhang Q, Liang J, Zhao L et al (2020) Synthesis of Novel Fluorescent Carbon Quantum Dots From for Rapid and Highly Selective Detection of o-nitrophenol and Cellular Imaging. *Front Chem* 8:665
22. Kou X, Jiang S, Park S-J, Meng L-Y (2020) A review: recent advances in preparations and applications of heteroatom-doped carbon quantum dots. *Dalton Trans* 49:6915–6938
23. Molaei MJ (2019) A review on nanostructured carbon quantum dots and their applications in biotechnology, sensors, and chemiluminescence. *Talanta* 196:456–478
24. Jelinek R (2016) *Carbon Quantum Dots: Synthesis, Properties and Applications*. Springer, Switzerland
25. Dong L, Zhang W, Li X, Geng X (2019) Preparation of CQDs with hydroxyl function for Fe³⁺ detection. *Micro & Nano Lett* 14:440–444
26. Jelinek R (2017) Characterization and Physical Properties of Carbon-Dots. *Carbon Nanostruc*:29–46
27. Chousidis I, Stalikas CD, Leonardos ID (2020) Induced toxicity in early-life stage zebrafish (*Danio rerio*) and its behavioral analysis after exposure to non-doped, nitrogen-doped and nitrogen, sulfur-co doped carbon quantum dots. *Environ Toxicol Pharmacol* 79: 103426
28. Hu Y, Guan R, Shao X et al (2020) Synthesis of Carbon Dots by Varying Doped Elements and Application in Serine Detection. *J Fluoresc*. <https://doi.org/10.1007/s10895-020-02592-1>
29. Gao R, Wu Z, Wang L et al (2020) Green Preparation of Fluorescent Nitrogen-Doped Carbon Quantum Dots for Sensitive Detection of Oxytetracycline in Environmental Samples. *Nanomaterials (Basel)* 10. <https://doi.org/10.3390/nano10081561>
30. Shi L, Zhou G, Xiang X et al (2020) Nitrogen-sulfur co-doped pH-insensitive fluorescent carbon dots for high sensitive and selective hypochlorite detection. *Spectrochim Acta A Mol Biomol Spectrosc* 242:118721
31. Omer KM, Tofiq DI, Hassan AQ (2018) Solvothermal synthesis of phosphorus and nitrogen doped carbon quantum dots as a fluorescent probe for iron(III). *Microchim Acta* 185:466
32. Wang Y, Hu X, Li W et al (2020) Preparation of boron nitrogen co-doped carbon quantum dots for rapid detection of Cr(VI). *Spectrochim Acta A Mol Biomol Spectrosc* 243:118807
33. Wang Y, Zhuang Q, Ni Y (2015) Facile Microwave-Assisted Solid-Phase Synthesis of Highly Fluorescent Nitrogen-Sulfur-Codoped Carbon Quantum Dots for Cellular Imaging Applications. *Chem Eur J* 21:13004–13011
34. Liang Q, Ma W, Shi Y et al (2013) Easy synthesis of highly fluorescent carbon quantum dots from gelatin and their luminescent properties and applications. *Carbon* 60:421–428
35. Hu X, An X, Li L (2016) Easy synthesis of highly fluorescent carbon dots from albumin and their photoluminescent mechanism and biological imaging applications. *Mater Sci Eng C* 58:730–736
36. Sahu S, Behera B, Maiti TK, Mohapatra S (2012) Simple one-step synthesis of highly luminescent carbon dots from orange juice: application as excellent bio-imaging agents. *Chem Commun* 48: 8835–8837
37. Mehta VN, Jha S, Kailasa SK (2014) One-pot green synthesis of carbon dots by using *Saccharum officinarum* juice for fluorescent imaging of bacteria (*Escherichia coli*) and yeast (*Saccharomyces cerevisiae*) cells. *Mater Sci Eng C Mater Biol Appl* 38:20–27
38. Zhang Z, Hao J, Zhang J et al (2012) Protein as the source for synthesizing fluorescent carbon dots by a one-pot hydrothermal route. *RSC Adv* 2:8599
39. Tang Q, Zhu W, He B, Yang P (2017) Rapid Conversion from Carbohydrates to Large-Scale Carbon Quantum Dots for All-Weather Solar Cells. *ACS Nano* 11:1540–1547
40. Magde D, Rojas GE, Seybold PG (1999) Solvent Dependence of the Fluorescence Lifetimes of Xanthene Dyes. *Photochem Photobiol* 70:737–744
41. Tadesse A, Hagos M, RamaDevi D et al (2020) Fluorescent-Nitrogen-Doped Carbon Quantum Dots Derived from Citrus Lemon Juice: Green Synthesis, Mercury (II) Ion Sensing, and Live Cell Imaging. *ACS Omega* 5:3889–3898
42. Pan L, Sun S, Zhang A et al (2015) Truly Fluorescent Excitation-Dependent Carbon Dots and Their Applications in Multicolor Cellular Imaging and Multidimensional Sensing. *Adv Mater* 27: 7782–7787
43. Pyrzyńska K, Pełka A (2013) Application of free radical diphenylpicrylhydrazyl (DPPH) to estimate the antioxidant capacity of food samples. *Anal Methods* 5:4288
44. Sachdev A, Gopinath P (2015) Green synthesis of multifunctional carbon dots from coriander leaves and their potential application as antioxidants, sensors and bioimaging agents. *Analyst* 140:4260–4269
45. Shi B, Su Y, Zhang L et al (2016) Nitrogen and Phosphorus Co-Doped Carbon Nanodots as a Novel Fluorescent Probe for Highly Sensitive Detection of Fe(3+) in Human Serum and Living Cells. *ACS Appl Mater Interfaces* 8:10717–10725
46. Chandra S, Laha D, Pramanik A et al (2016) Synthesis of highly fluorescent nitrogen and phosphorus doped carbon dots for the detection of Fe(3+) ions in cancer cells. *Luminescence* 31:81–87
47. Atchudan R, Jebakumar TN, Aseer KR et al (2018) Highly fluorescent nitrogen-doped carbon dots derived from *Phyllanthus acidus* utilized as a fluorescent probe for label-free selective detection of Fe³⁺ ions, live cell imaging and fluorescent ink. *Biosens Bioelectron* 99:303–311
48. Ramezani Z, Qorbanpour M, Rahbar N (2018) Green synthesis of carbon quantum dots using quince fruit (*Cydonia oblonga*) powder as carbon precursor: Application in cell imaging and As³⁺ determination. *Colloids Surf A Physicochem Eng Asp* 549:58–66

49. Fernando KAS, Sahu S, Liu Y et al (2015) Carbon quantum dots and applications in photocatalytic energy conversion. *ACS Appl Mater Interfaces* 7:8363–8376
50. Molaei MJ (2020) The optical properties and solar energy conversion applications of carbon quantum dots: A review. *Sol Energy* 196:549–566
51. Gu D, Shang S, Yu Q, Shen J (2016) Green synthesis of nitrogen-doped carbon dots from lotus root for Hg (II) ions detection and cell imaging. *Appl Surf Sci* 390:38–42
52. Liu Y, Liu Y, Park M et al (2017) Green synthesis of fluorescent carbon dots from carrot juice for in vitro cellular imaging. *Carbon Lett* 21:61–67
53. Carvalho J, Santos LR, Germino JC et al (2019) Hydrothermal Synthesis to Water-stable Luminescent Carbon Dots from Acerola Fruit for Photoluminescent Composites Preparation and its Application as Sensors. *Mater Res* 22
54. Zhu S, Meng Q, Wang L et al (2013) Highly photoluminescent carbon dots for multicolor patterning, sensors, and bioimaging. *Angew Chem Int Ed Eng* 52:3953–3957
55. Dong Y, Pang H, Yang HB et al (2013) Carbon-based dots co-doped with nitrogen and sulfur for high quantum yield and excitation-independent emission. *Angew Chem Int Ed Eng* 52: 7800–7804
56. Hao A, Guo X, Wu Q et al (2016) Exploring the interactions between polyethyleneimine modified fluorescent carbon dots and bovine serum albumin by spectroscopic methods. *J Lumin* 170:90–96
57. Singh R, Yadav A, Shekhar S et al (2019) Nitrogen Doped Carbon Quantum Dots Modified by *Lens culinaris* β -Galactosidase as a Fluorescent Probe for Detection of Lactose. *J Fluoresc* 29:1213–1219
58. Trivedi MK, Trivedi ABD (2015) Spectroscopic Characterization of Disodium Hydrogen Orthophosphate and Sodium Nitrate after Biofield Treatment. *J Chromatogr Sep Tech* 06
59. Rahmani Z, Ghaemy M (2019) One-step hydrothermal-assisted synthesis of highly fluorescent N-doped carbon dots from gum tragacanth: Luminescent stability and sensitive probe for Au³⁺ ions. *Opt Mater* 97:109356
60. Zhang Z, Sun W, Wu P (2015) Highly Photoluminescent Carbon Dots Derived from Egg White: Facile and Green Synthesis, Photoluminescence Properties, and Multiple Applications. *ACS Sustain Chem Eng* 3:1412–1418
61. Yan Z, Shu J, Yu Y et al (2015) Preparation of carbon quantum dots based on starch and their spectral properties. *Luminescence* 30: 388–392
62. Omer KM (2018) Highly passivated phosphorous and nitrogen co-doped carbon quantum dots and fluorometric assay for detection of copper ions. *Anal Bioanal Chem* 410:6331–6336
63. Huang Y, Zhang Y, Yan Z, Liao S (2015) Assay of ceftazidime and cefepime based on fluorescence quenching of carbon quantum dots. *Luminescence* 30:1133–1138
64. Shen T-Y, Jia P-Y, Chen D-S, Wang L-N (2021) Hydrothermal synthesis of N-doped carbon quantum dots and their application in ion-detection and cell-imaging. *Spectrochim Acta A Mol Biomol Spectrosc* 248:119282
65. (2017) Fluorescence switching sensor for sensitive detection of sinapine using carbon quantum dots. *Sensors Actuators B Chem* 241:482–488
66. Dhenadhayalan N, Lin K-C (2015) Chemically induced fluorescence switching of carbon-dots and its multiple logic gate implementation. *Sci Rep* 5:10012
67. Das B, Dadhich P, Pal P et al (2014) Carbon nanodots from date molasses: new nanolights for the in vitro scavenging of reactive oxygen species. *J Mater Chem B Mater Biol Med* 2:6839–6847

Publisher's Note Springer Nature remains neutral with regard to jurisdictional claims in published maps and institutional affiliations.